Reliable NMR chemical shifts for molecules in solution by methods rooted in density functional theory

ARTICLE *in* MAGNETIC RESONANCE IN CHEMISTRY · OCTOBER 2004

Impact Factor: 1.18 · DOI: 10.1002/mrc.1447 · Source: PubMed

4 AUTHORS, INCLUDING:

Michele Pavone
University of Naples Federico II
58 PUBLICATIONS **1,181** CITATIONS
SEE PROFILE

Vincenzo Barone
Scuola Normale Superiore di Pisa
773 PUBLICATIONS **44,577** CITATIONS
SEE PROFILE

MAGNETIC RESONANCE IN CHEMISTRY
Magn. Reson. Chem. 2004; **42**: S57–S67
Published online in Wiley InterScience (www.interscience.wiley.com). DOI: 10.1002/mrc.1447

Reliable NMR chemical shifts for molecules in solution by methods rooted in density functional theory†

Caterina Benzi, Orlando Crescenzi, Michele Pavone and Vincenzo Barone*

Dipartimento di Chimica, Università Federico II, Complesso Universitario di Monte S. Angelo, Via Cintia, I-80126 Naples, Italy

Received 19 March 2004; Revised 12 May 2004; Accepted 12 May 2004

The conceptual and numerical problems involved in the computation of reliable NMR chemical shifts for molecules in condensed phases are analyzed with reference to a number of case studies ranging from aromatic compounds in low-polarity solvents to carbonyl and amidic models in aqueous solution and to large polypeptides. The results show that an integrated tool including the most recent density functionals, mixed discrete-continuum solvent models, hybrid QM/MM approaches and, when needed, averaging from molecular dynamics simulations are becoming an invaluable complement to experimental results.

KEYWORDS: NMR; chemical shifts; solution; density functional theory

INTRODUCTION

NMR spectroscopy is nowadays the technique of choice for the structural characterization of molecules in solution. Among many measurable parameters, chemical shifts (δ) are particularly sensitive to molecular composition, conformation and environment. Although well-established empirical rules have been used in the past to describe and interpret the fine tuning of chemical shifts by several short- and long-range effects even for large molecules,[1–3] a more powerful tool has been developed in recent years based on quantum mechanical computations.[4,5] Methods rooted in density functional theory (DFT)[6] are particularly appealing in this connection, since they couple remarkable accuracy with a favorable scaling with the number of active electrons.[7–10] We shall make special reference to the so called hybrid functionals, in which some Hartree–Fock (HF) exchange is mixed with its local counterpart.[7]

Some years ago, it was pointed out that for organic molecules the MP2 model outperformed all the current DFT approaches, including the widely used B3LYP hybrid model.[8] However, the development of new functionals[11,12] is changing the situation. In particular, a benchmark study on small molecules[13] has shown that the PBE0 hybrid model,[11] which does not contain any adjustable parameter, performs very well for ^{13}C and ^{15}N nuclei, irrespective of their hybridization state. The situation is less satisfactory for ^{17}O, although the reliability of PBE0, in contrast to B3LYP, is close to that of MP2. As already found for electron spin resonance (ESR),[14] the chemical shifts of hydrogen atoms are reproduced reasonably well by several functionals. In any case, Fig. 1 shows that the quality of the results delivered by the PBE0 functional is largely sufficient for a reliable assignment of experimental spectra.

Starting from this point, we will analyze in the following sections the additional aspects that play a role in the computation of chemical shifts for molecules in condensed phases. After a sketch of the building blocks of a comprehensive computational tool, we will analyze in sequence the reliability of DFT results for medium-sized molecules in low-polarity solvents, the role of vibrational averaging effects, the proper inclusion of solvent effects and the use of mixed quantum/classical methods for the study of local properties in very large systems.

METHODS

All the calculations of nuclear shielding tensors were carried out with the Gaussian 03 suite of programs[15] using the GIAO approach:[8]

$$\sigma_{ji} = \left[\frac{\partial^2 E}{\partial B_i \partial \mu_j}\right] = \sum_{\alpha\beta} D_{\alpha\beta} \frac{\partial^2 h_{\alpha\beta}}{\partial B_i \partial \mu_j} + \sum_{\alpha\beta} \frac{\partial D_{\alpha\beta} \partial h_{\alpha\beta}}{\partial B_i \partial \mu_j}$$

where σ_{ji} is the jith component of the shielding tensor, B_i is the ith component of the external magnetic field and μ_j is the jth component of the nuclear magnetic moment; $D_{\mu\nu}$ and $h_{\mu\nu}$ are generic elements of the one-electron density and Hamiltonian matrix, respectively in the GIAO basis. The isotropic shielding (σ) is defined as one-third of the trace of the shielding tensor; the chemical shift δ is computed as $\delta_{\text{sample}} = \delta_{\text{ref}} + \sigma_{\text{ref}} - \sigma_{\text{sample}}$, where δ_{sample}, σ_{sample} refer to the compound under study, δ_{ref} is the experimental chemical shift for a suitable reference system and σ_{ref} is the corresponding computed isotropic shielding.

†Dedicated to Professor M. Barfield on the occasion of his 70th birthday.

*Correspondence to: Vincenzo Barone, Dipartimento di Chimica, Università Federico II, Complesso Universitario di Monte S. Angelo, Via Cintia, I-80126 Naples, Italy. E-mail: baronev@unina.it
Contract/grant sponsor: Ministry of Instruction, University and Research (MIUR).

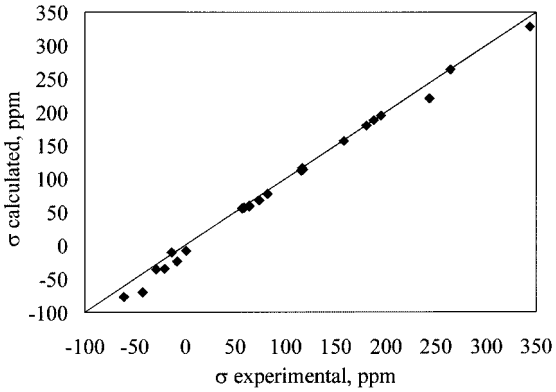

Figure 1. Comparison between calculated (PBE0) and experimental absolute shieldings for ^{13}C, ^{15}N and ^{17}O atoms of 32 small molecules.

The quantum mechanical methods employed in the present work range from Hartree–Fock (HF) to different models rooted in DFT.[6,7] Most of the computations were performed using the PBE0 model,[11] in which the gradient-corrected Perdew–Burke–Ernzerhof (PBE) exchange and correlation functionals[16] are combined with a fixed amount (25%) of HF exchange. Some comparisons were made with the more widely used B3LYP model, in which the Becke exchange and Lee–Yang–Parr correlation functionals are combined with their local and HF counterparts by means of three optimized parameters.[17] Polarized double and triple ζ basis sets of the Pople series augmented by diffuse functions[18] were generally used, but their convergence was tested in some cases also with reference to correlation consistent basis sets.[19]

Solvent effects were taken into account by different approaches; bulk solvent effects were described by the latest version of the polarizable continuum model (PCM).[20,21] In this approach, the solute molecule is embedded in a cavity formed by the envelope of spheres centered on solute atoms or atomic groups; inside the cavity the relative dielectric constant is equal to 1 as in vacuum, whereas it takes the solvent bulk value outside the cavity. The solvent is polarized by the presence of the solute molecule; such a polarization creates a reaction field that is described in terms of effective charges on the cavity surface. Thus the solute molecular Hamiltonian is perturbed by a reaction field operator

$$\hat{H} = \hat{H}^0 + \hat{V}_{RF}$$

$$\hat{V}_{RF} = \frac{1}{2}\int_{\text{surface}} \phi(\mathbf{r}')D(\mathbf{r}', \mathbf{r})\phi(\mathbf{r})\mathrm{d}\mathbf{r}'\mathrm{d}\mathbf{r}$$

where $\hat{H}^0$ is the Hamiltonian of the isolated molecule, $\phi(\mathbf{r})$ is the electrostatic potential on the cavity surface and $D(\mathbf{r}', \mathbf{r})$ is a function depending on cavity geometry and solvent dielectric constant. Starting from this definition, very effective linear scaling procedures have been implemented for cavity construction and evaluation of energy and of its first and second derivatives with respect to geometric, electric and magnetic parameters.[21]

Ab initio molecular dynamics were carried out within the Car–Parrinello (CP) method,[22] which is based on an extended Lagrangian molecular dynamics (MD) scheme where the potential energy surface is computed at the DFT level: in order to decrease the demanding computational cost, the electronic degrees of freedom are propagated, together with the nuclear ones, as dynamic variables, with fictitious masses. The CP-MD simulations were performed by a parallel version[23] of the original CP code,[24] using the PBE functional and expanding the wavefunctions in plane waves up to an energy cut-off of 25 Ry. We also employed the atom-centered density matrix propagation (ADMP) method,[25] a recent extension of the original CP approach, in which the propagation of the density matrix allows the use of atom-centered functions to form the basis sets of the simulations. The ADMP molecular dynamics were carried out with the B3LYP functional and Gaussian basis sets using the Gaussian 03 package.

Classical molecular dynamics simulations were carried out with the SANDER module of the AMBER6 package[26] using the 1994 AMBER force field.[27]

Systems too large for a brute-force quantum mechanical (QM) description were treated by a hybrid approach in which the system is subdivided into several parts or layers treated at different levels of theory. The most important part of the system, i.e. the region where the local phenomena in which we are interested take place, forms the model system and is described at the higest level of theory, whereas subsequent layers are described with progressively less accurate methods, i.e. lower-level QM models or Molecular Mechanics (MM). We chose to employ the ONIOM scheme,[28] performing PBE0//HF//AMBER computations with the so-called 'electronic embedding'[29] scheme, namely including the point charges of the MM layer in the QM Hamiltonian of the model system according to the scheme

$$\hat{H}_{el}(\text{model:MM}) = \hat{H}_{el}(\text{model}) - \sum_{i}^{Y}\sum_{J}^{X}\frac{q_J}{r_{ij}}$$

where $\hat{H}_{el}$ (model : MM) and $\hat{H}_{el}$ (model) are the electronic Hamiltonians for the QM region with and without the external field, Y is the number of the electrons in the model systems and X that of the point charges in the MM region.

RESULTS AND DISCUSSION

Medium-sized molecules

As an example of the kind of organic compounds which are amenable to chemical shift calculations,[30] let us consider 3*H*-phenoxazin-3-one (**1**), 5*H*-pyrido[3,2-a]phenoxazin-5-one (**2**) and 5*H*-pyrido[2,3-a]phenoxazin-5-one (**3**) (Scheme 1).

Table 1 gives a comparison of the performances of PBE0 and B3LYP functionals during the NMR calculations: the two functionals are essentially equivalent in the prediction of proton shifts, whereas for carbon shifts the PBE0 results are slightly closer to the experiment, the difference being mostly related to a better agreement for quaternary ring-junction atoms.

Apparently (Table 2), adoption of basis sets larger than 6–311+G(d,p) does not significantly improve the agreement with the experimental results.

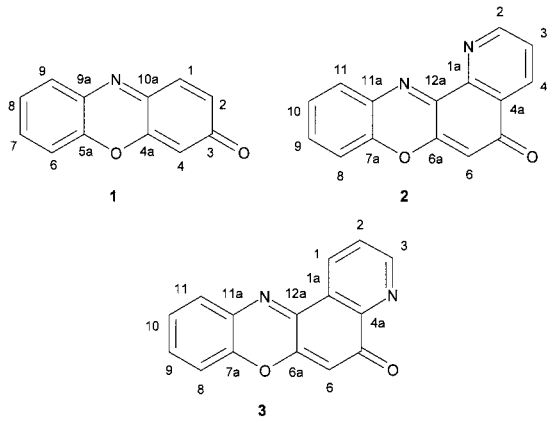

Scheme 1. Structural formulae and atom numbering of 3*H*-phenoxazin-3-one (**1**), 5*H*-pyrido[2,3-a]phenoxazin-5-one (**2**) and 5*H*-pyrido[3,2-a]phenoxazin-5-one (**3**).

Table 1. Comparison of the PBE0 and B3LYP functionals in the prediction of chemical shifts, as judged by RMSDs between experimental and computed shifts (ppm) [all NMR calculations use the 6–311+G(d,p) basis set and PBE0/6–31G(d) geometries]

	^{1}H		^{13}C			
Compound	PBE0	B3LYP	PBE0, all	PBE0, ring junction	B3LYP, all	B3LYP, ring junction
1	—	—	1.35	1.20	1.44	1.72
2	0.18	0.18	1.16	0.86	1.35	1.48
3	0.23	0.22	1.36	1.33	1.44	1.66

Hence the final carbon and proton spectra of the three heterocyclic systems (and also of several ring-substituted derivatives) were calculated at the PBE0/6–311+G(d,p)//PBE0/6–31G(d) level (Table 3). Figure 2 depicts the usual linear correlation plots between computed and experimental values of the carbon chemical shift for the parent 3*H*-phenoxazin-3-one ring system (compound **1**, Scheme 1): the agreement is fairly good and actually typical of the whole series, allowing in most cases unambiguous confirmation of the experimental assignments.

The choice of the reference compound for conversion of the computed isotropic shieldings to chemical shifts deserves some comment. If possible, it is of advantage to use as the reference an atom that is chemically similar to the nuclei in which one is interested; in fact, using benzene as the reference compound, the cancellation of systematic errors for the case of the essentially aromatic phenoxazones and pyridophenoxazones was so good that even recourse to linear correlation procedures[30] was unnecessary, and the computed chemical shifts could be used directly.

Table 3. Observed and calculated ^{1}H and ^{13}C NMR chemical shifts (δ, ppm) for the three parent ring systems, compounds **1**, **2** and **3**

	1		**2**		**3**	
Atom	Calc.	Expt.[a]	Calc.	Expt.[b]	Calc.	Expt.[b]
H-1	7.30	—			9.12	9.10
H-2	6.56	—	8.98	9.16	7.37	7.74
H-3			7.47	7.71	9.02	9.12
H-4	6.07	—	8.78	8.64		
H-6	7.19	—	6.25	6.51	6.28	6.66
H-7	7.36	—				
H-8	7.21	—	7.20	7.36	7.22	7.39
H-9	7.75	—	7.40	7.57	7.34	7.56
H-10			7.27	7.41	7.21	7.40
H-11			8.01	8.12	7.79	7.88
C-1	135.1	135.2			133.3	133.1
C-1a			147.5	147.2	126.9	127.9
C-2	137.0	134.8	153.5	153.4	124.0	126.1
C-3	184.3	186.4	125.0	125.9	154.6	153.4
C-4	106.7	107.0	135.6	134.1		
C-4a	148.0	149.7	128.5	128.6	147.8	147.2
C-5			180.8	182.2	179.5	182.3
C-5a	144.5	144.0[c]				
C-6	116.2	116.2	105.4	106.8	108.6	108.6
C-6a			151.4	152.0	149.3	151.0
C-7	131.1	132.8				
C-7a			144.0	143.9	144.6	144.1
C-8	125.5	125.5	116.0	115.7	116.4	116.2
C-9	132.8	130.5	132.9	132.5	132.3	132.4
C-9a	134.4	133.4				
C-10			125.1	125.5	124.8	125.6
C-10a	150.2	148.8[c]				
C-11			133.9	131.0	131.7	130.1
C-11a			134.4	132.8	133.3	132.6
C-12a			147.5	146.4	148.7	146.3

[a] Ref. 31.

[b] Ref. 32.

[c] Assignments swapped with respect to literature reference.

Table 2. Basis set convergence in the prediction of chemical shifts, as judged by RMSDs between experimental and computed shifts (ppm) [all NMR calculations use the PBE0 functional and PBE0/6–31G(d) geometries]

	^{1}H				^{13}C			
Compound	6–311+G (d,p)	6–311+G (2d,2p)	6–311++G (2d,2p)	6–311+G (2df,2p)	6–311+G (d,p)	6–311+G (2d,2p)	6–311++G (2d,2p)	6–311+G (2df,2p)
1	—	—	—	—	1.35	1.38	1.37	1.40
2	0.18	0.16	0.17	0.15	1.16	1.17	1.17	1.24
3	0.23	0.20	0.20	0.19	1.36	1.44	1.45	1.52

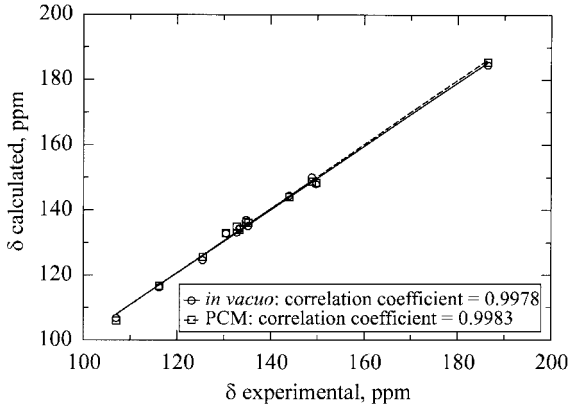

Figure 2. Experimental carbon shifts for 3*H*-phenoxazin-3-one (**1**, Scheme 1) in $CDCl_3$ compared with the values computed *in vacuo* and in the presence of a polarizable solvent model (PCM) mimicking $CDCl_3$.

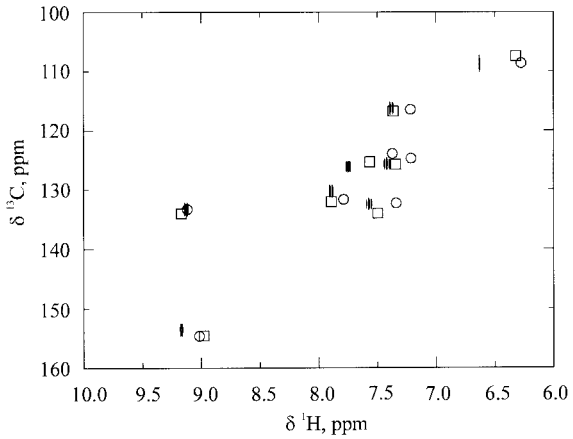

Figure 3. Experimental and calculated [PBE0/6–311+G(d,p)//PBE0/6–31G(d)] carbon–proton one-bond correlation spectrum of 5*H*-pyrido[3,2-a]phenoxazin-5-one. Circles, *in vacuo* calculation; squares, $CDCl_3$ solvent simulated by the PCM model.

Calculation of spectroscopically useful shieldings is definitely more difficult for protons than for carbons, since the reduced spectral dispersion typical of proton spectra makes even a small (a couple of tenths of ppm) error comparatively significant.

However, the combined use of computed proton and carbon shifts can be exploited for interpretation of CH-correlation spectra: thus, for example, Fig. 3 compares the simulated and the experimental one-bond correlation spectrum of **3**.

The rather apolar nature of the compounds, and also of the solvent used during the collection of spectra ($CDCl_3$), made solvent effects fairly small in this instance. For comparison, Fig. 2 also shows the linear correlation obtained by use of the PCM during the GIAO NMR calculation, and the improvement with respect to the *in vacuo* results is only marginal. However, this is not necessarily the case for more polar solutes/solvents, or for different nuclei.

Before discussing in more detail the issue of solvent effects, it may be of interest to examine briefly some

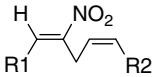

6: R1 = -$(CH_2)_6$COOEt, R2 = -$(CH_2)_3CH_3$
7: R1 = -$(CH_2)_3CH_3$, R2 = -$(CH_2)_6$COOEt
10: R1 = R2 = CH_3

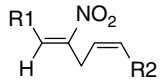

8: R1 = -$(CH_2)_6$COOEt, R2 = -$(CH_2)_3CH_3$
9: R1 = -$(CH_2)_3CH_3$, R2 = -$(CH_2)_6$COOEt
11: R1 = R2 = CH_3

Scheme 2. Structural formulae of linoleic acid nitration products and of the simplified models used in the NMR calculations.

results for ^{15}N. Again, instead of trying to calculate quantitative absolute shielding constants, for the usual chemical applications it is convenient to concentrate on the much easier task of obtaining accurate chemical shifts, where an appropriate choice of the reference compound can be of great help. In connection with some biomimetic studies on the nitrite-induced nitration of linoleic acid derivatives,[33] nitroalkenes **6**–**9** (Scheme 2) were isolated, and the ^{15}N chemical shifts of the nitro groups were determined after isotopic labeling. In order to substantiate the structural assignments, it was of interest to compute independently the ^{15}N chemical shifts. In this case, the obvious choice for the reference compound to adopt in the computational protocol was nitromethane. However, the size and the flexibility of the molecules made calculations on the whole structures unattractive, and the model compounds **10** (for **6** and **7**) and **11** (for **8** and **9**) were used instead.

Even after this simplification, exploration of the potential energy surfaces of **10** and **11** was still the bottleneck of the whole calculation: for instance, conformational analysis of **10** required 18 PBE0/6–31G(d) geometry optimizations, leading to identification of two conformers of comparable energy (Fig. 4). Separate NMR computations [GIAO, PBE0/6–311+G(d,p)] were performed on each of these geometries, and the resulting shieldings were averaged according to a Boltzmann distribution: the resulting computed ^{15}N chemical shift (376.3 ppm) matches the experimental value of 377.5 ppm fairly well. The analogous procedure applied to the 2*Z*,5*Z*-isomer **11** produced similar good agreement with experiment (380.3 vs 380.5/380.9 ppm for **8** and **9**). Again, computed proton shifts were best used in combination with the comparatively more accurate heteronuclear shifts, namely to interpret N–H long-range correlation spectra.

Table 4 reports some significant measured (two-dimensional heteronuclear multiple bond correlation experiments) correlations for **6**–**9** (illustrated pictorially in Fig. 4), along with the calculated proton and nitrogen shifts.

Vibrational averaging effects

All calculations reported so far have been carried out on one or several minimum energy conformations of the molecules: this amounts to neglecting vibrational averaging effects completely. The question thus arises of how one could introduce this further degree of accuracy in the

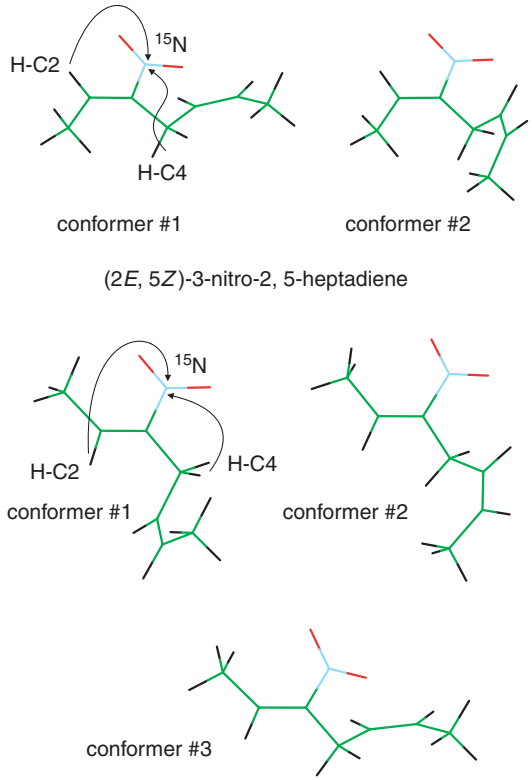

Figure 4. Minimum energy conformers of the isomeric model compounds **10** and **11**. The arrows highlight significant N–H multiple-bond correlations.

Table 4. Comparison of experimental and calculated values of selected chemical shifts for compounds **6–9**

Compound	Nucleus	δ expt. (ppm)[a]	δ calc. (ppm)
(2*E*,5*Z*)-3-Nitro-2,5-heptadiene	H–C2	7.08–7.12	7.454
	H–C4	3.33–3.27	3.103
	N	377.5–377.5	376.31
(2*Z*,5*Z*)-3-Nitro-2,5-heptadiene	H–C2	5.72–5.65	6.125
	H–C4	3.25–3.30	3.045
	N	380.5–380.9	380.30

[a] Pairs of experimental values are for the isomeric linoleic acid derivatives **6**/**7** and **8**/**9**.

calculation of NMR parameters. In fact, there are several possibilities, which range in accuracy from the full quantum-mechanical treatment of nuclear motions in the anharmonic vibrational potential[34,35] to simpler procedures rooted in classical mechanics. For semi-rigid molecules in the gas phase, the most straightforward QM approach is based on second-order perturbation theory. At this level the vibrationally averaged value of a property P at 0 K is given by[36]

$$\langle P\rangle_0 = P_{eq} + 0.25\sum_k \left(P''_{kk} - \sum_l P'_l F_{kll}/\omega_k\omega_l \right) /\omega_k$$

where P'_k and P''_{kk} are first and second derivatives of the property with respect to normal modes, ω_k, ω_l are harmonic frequencies and F_{kll} third energy derivatives with respect to normal modes. The harmonic approximation is recovered neglecting the term involving first derivatives of the property. This procedure is being applied in a number of studies for small- and medium-sized molecules in gas phase with encouraging results.[37]

Another approach that is becoming increasingly popular is based on classical dynamics using *ab initio* potentials (e.g. Car–Parrinello).[22] Of course, the strength of the method is mostly apparent in the simulation of molecules in solution: nonetheless, some examples for isolated molecules can also be discussed. Table 5 reports the ^{17}O and ^{13}C absolute shieldings [at the PBE0/6–311+G(d,p) level] for the acetone molecule *in vacuo*, either computed on single equilibrium geometries, or averaged over 40 frames extracted from a 4.0 ps plane-waves Car–Parrinello simulation carried out with the PBE density functional. For the rather rigid carbonyl group of acetone, the vibrational effect on average shieldings is fairly small, whereas the variance during the dynamics is large: in part this may be due to an overestimation of vibrational amplitudes connected with the classical description of nuclear motion.[35,37]

However, when large-amplitude motions are active, results from the dynamics simulations can contain a wealth of information not available from simple computations on equilibrium structures. To illustrate this difference on the basis of the NMR behaviour of still another nucleus, let us consider the case of a fluxional compound, SF_4.[38] The molecule has a slightly distorted trigonal bipyramidal structure, with one vacant equatorial position, hence two sets of non-equivalent fluorine atoms exist. However, the interchange between axial and equatorial fluorines is fairly rapid at room temperature [the experimental activation free energy is 12.2 kcal mol^{-1} (1 kcal = 4.184 kJ) in the gas phase[39]]. During the interconversion mechanism, known as Berry pseudorotation, the pair of axial fluorines is converted into the pair of equatorial fluorines by way of a transition state corresponding to a square bipyramidal arrangement (Scheme 3).

All four fluorine atoms are equivalent in the transition structure; hence NMR calculations of ^{19}F chemical shifts can easily be used to follow the axial–equatorial interconversion during the course of an *ab initio* dynamics. The presence of the sulfur atom required some benchmarking for an optimal choice of the basis set, for both energy and property evaluations. Although the 6–311+G(2d) basis set performs

Table 5. Comparison of NMR parameters of the acetone molecule computed *in vacuo* by different approaches

Geometry	Carbonyl ^{17}O σ (ppm)	Carbonyl ^{13}C σ (ppm)
PBE/plane waves minimum	−367.5	−26.6
PBE/6–31+G(d,p) minimum	−366.7	−26.6
Average over Car–Parrinello simulation	−374.2 ± 46.2	−28.8 ± 11.9

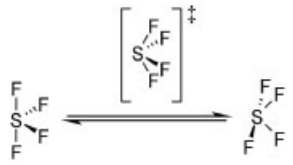

Scheme 3. Schematic representation of the Berry pseudorotation of SF_4.

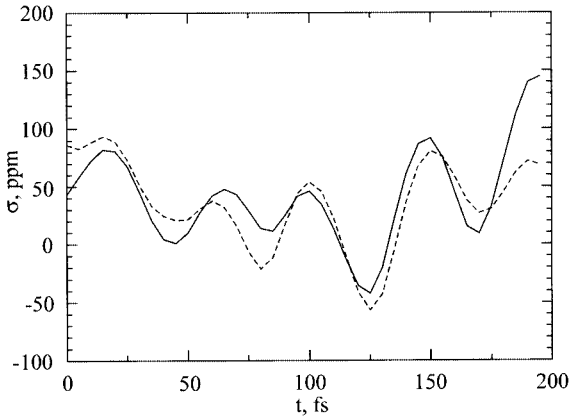

Figure 5. Computed absolute ^{19}F shieldings along the high-temperature (550 K) ADMP trajectory. Continuous line, initially equatorial fluorine pair; dashed line, initially axial fluorine pair.

well in the computation of chemical shifts, a reasonable activation energy could be computed only by using at least a 6–311G(3df) basis set for sulfur. At this level, the computed activation free energy for the Berry pseudorotation is 11.1 kcal mol^{-1}, which was deemed sufficiently close to the experimental value to reflect the reaction kinetics accurately. The actual dynamics simulations were carried out within the atom-centered density matrix propagation (ADMP) formalism.[25] Figure 5 shows the ^{19}F absolute shieldings, computed at the B3LYP/6–311+G(2d) level on a number of snapshots extracted from a high-temperature (550 K) dynamics; only two curves are shown, since the values for the two interconverting axial–equatorial fluorine pairs have been averaged for the sake of clarity. The crossing points between the two curves correspond to several passages through the transition state, and imply equivalence of the fluorines.

A second ADMP run carried out around room temperature (where the experimental chemical shifts of the two fluorine pairs remain distinct) did not give any evidence of Berry pseudorotation. Furthermore, the computed chemical shift difference between axial and equatorial fluorines, averaged along the whole dynamics, was 59.0 ppm, in close agreement with the experimental value of 60.9 ppm.

Solvent effects

All the cases discussed above concerned chemical shifts of apolar molecules in the gas phase or in low-polarity solvents, and therefore have been aptly tackled by *in vacuo* calculations: however, in a more general perspective, solvent effects on NMR spectra can be of considerable size, and it is of fundamental importance to evaluate environmental effects on NMR parameters at a comparable quantitative level. In recent years, essentially three different approaches have been proposed and employed: continuum solvent models, discrete clusters and molecular dynamics (either classical or *ab initio*).[40,41] In order to illustrate their relative merits, the solvation shift on the isotropic ^{17}O shielding for some simple test molecules will be discussed in some detail. Apart from the availability of suitable experimental data, the choice was motivated by the unusually large solvation shifts which are observed in connection with the direct involvement of oxygen in hydrogen bonds. Moreover, as will be discussed below, some limitations of the continuum solvent models emerged, e.g. in the case of aqueous solutions, which called for a comparison with alternative approaches.

In general, however, it is fair to state that the most convenient way to account for solvation effects on NMR parameters (and also on several other molecular properties) is represented by a suitable continuum solvent model: as mentioned in the Methods section, in all cases discussed here, the well-known polarizable continuum model (PCM) was adopted.[20,21] Concerning specifically NMR parameters, the PCM description affects the computation at several levels: in the first place, the reaction field alters both the equilibrium geometry and the electronic distribution of the solute; moreover, inclusion of the PCM operator introduces additional terms in the GIAO differentiation. It should be noted that in principle changes in the solute vibrational motion can also be taken into account within the PCM procedure;[14] however, this level of detail was not actually pursued in the examples discussed here.

Figure 6 shows the relative solvent shifts for the carbonyl ^{17}O of *N*-methylformamide (with respect to the shift in CCl_4, the least polar medium explored) computed by PCM alone in different solvents: it is apparent that the values computed for aprotic solvents (toluene, acetone, acetonitrile, DMSO) of increasing dielectric constant fall on a smooth curve and, by proper scaling of the atomic radii used to build the cavity occupied by the solute in the dielectric medium, can be made to correspond closely to experiment; by contrast, solvation shifts computed for solvents capable of forming hydrogen bonds with the carbonyl oxygen ($CHCl_3$, ethanol, methanol, water) are much too small. Hence, at least in the very demanding case of ^{17}O, PCM is unable to reproduce fully the effect of solvent hydrogen bonding on chemical shift.

The natural alternative is to include the strongly bound solvent molecules explicitly, i.e. to carry out the whole calculation on a cluster. A first difficulty in this approach lies in choosing the correct number of solvent molecules to be included in the cluster; moreover, even if one settles on a definite cluster size, in general there will be many accessible geometries, which will need to be averaged in the NMR calculation. Another issue is that of long-range effects: for solvents such as water, the hydrogen bonding network around the solute is so extended that it would take a very large cluster to account for the (sizeable) bulk solvent influence. Fortunately, however, the PCM model can again be brought into play: one simply needs to treat the (small) cluster as a sort of supermolecule, building the PCM cavity around it,

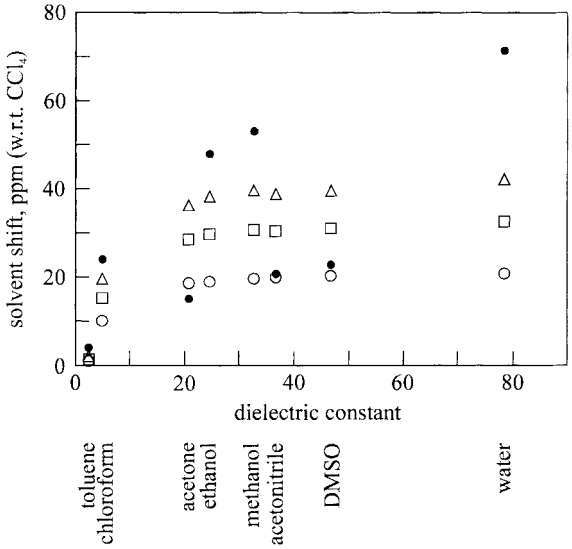

Figure 6. Relative solvent shifts (with respect to CCl_4) on the ^{17}O chemical shift of *N*-methylformamide. Closed circles, experimental values; open circles, PCM with radii scaling factor of 1.4; squares, PCM with radii scaling factor of 1.2; triangles, PCM with radii scaling factor of 1.1.

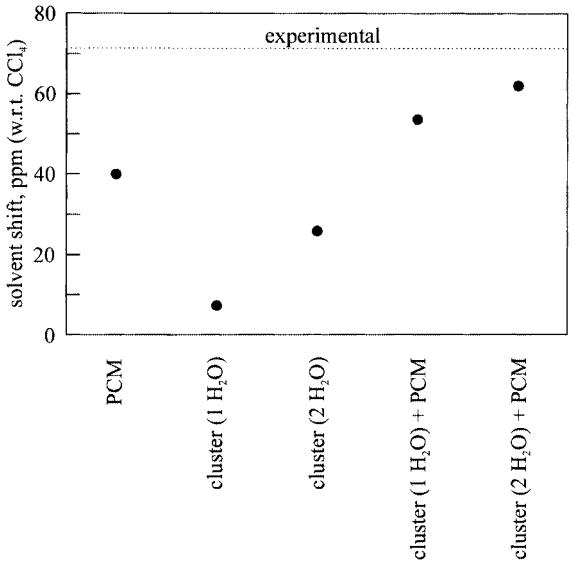

Figure 7. Relative solvent shifts (with respect to CCl_4) on the ^{17}O chemical shift of *N*-methylformamide, computed with different continuum, cluster and mixed solvent models.

and applying the usual PCM treatment. Figure 7 summarizes the results obtained by such cluster calculations for the solvation (CCl_4 to water) shift of *N*-methylformamide ^{17}O: the (geometry optimized) clusters of solute plus one or two water molecules are by themselves unable to reproduce the experimental value; fairly satisfactory agreement is reached only by introduction of the PCM along with two explicit water molecules.

As hinted at above, in general it is difficult to gauge *a priori* the number of solvent molecules and the geometries to adopt in such a 'mixed' minimized cluster/PCM description. The issue can be approached by standard sampling techniques (Monte Carlo or molecular dynamics), carried out either at the level of classical force field simulations or even at the quantum mechanical level (Born–Oppenheimer, Car–Parrinello or ADMP dynamics[42]). The properties can be computed on the fly[43] or by post-processing of selected frames.[44,45]

To illustrate a possible approach, let us consider the solvation (vacuum to water) shift for acetone ^{17}O. In a first step, solvent configurations were sampled by classical dynamics, with a standard TIP3P model[46] for the water solvent, and parameters for the acetone molecule were taken from the AMBER force field.[27] The issue of force field quality would be crucial if the internal motions of the solute molecule were left free: therefore, the solute was kept frozen during the dynamics. In the present instance, the structure chosen was that obtained from a PBE0/6–31+G(d,p) optimization with the water solvent simulated by the PCM model. Of course, the choice of the actual geometry may not be unequivocal: e.g. one could have chosen the geometry resulting from QM optimization of an acetone-water(s) cluster, maybe using again PCM to account for the bulk. However, the important point is that the different choices affect the computed solvation shifts through a second-order effect, while the primary effect lies in the solvent–solute and solvent–solvent interactions sampled by the dynamics.

The obvious advantage of using classical force fields is that the computational cost required for long simulation times of even fairly large solvent boxes is comparatively insignificant. The actual *ab initio* calculation of NMR parameters takes place in a subsequent, separate stage, on selected snapshots extracted from the dynamics. In this connection, each single snapshot should be regarded as a huge static solute–solvent cluster: since we are interested in the spectroscopic properties of the 'central' solute molecule, the cluster can be trimmed down to include only a reasonable number of solvent molecules closest to the solute. In practice, it is easy to define an appropriate cluster size, by examining on a test set of frames the convergence of NMR parameters calculated for larger and larger clusters. Since this exploration involves calculations on large clusters, it may be sensible to carry it out with a smaller basis set. Figure 8 shows such a plot for the acetone–water system; for comparison, the corresponding results obtained by cluster–PCM calculations are also shown, together with average values computed at this level on 40 frames. A crucial point to note is that PCM can again be used to great advantage to describe accurately the major portion of the solvent, except for only the few water molecules closest to the acetone oxygen. In other words, in the absence of the PCM model it takes a very large cluster of explicit water molecules to reach convergence on the computed solvent shifts; by contrast, the same results are reproduced if one retains only the 2–5 proximal explicit waters (at the positions resulting from the dynamics) and introduces the PCM description.

Once the minimal required cluster size has been defined by the above procedure, the actual NMR computation employing a large basis set can be carried out: Fig. 9 shows the results at the PBE0/6–311+G(d,p) level, again with and without the use of the PCM model.

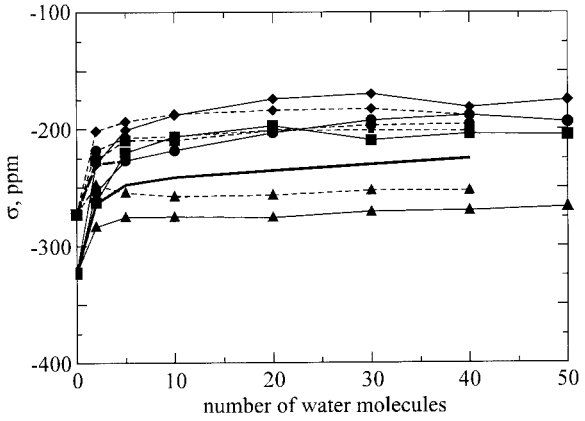

Figure 8. Acetone absolute ^{17}O shielding computed at the PBE0 level with a small basis set [6–31G(d)] on frames extracted from classical dynamics, as a function of the number of explicit water molecules retained in the NMR calculation. Full lines, NMR calculated *in vacuo* on the acetone–water clusters; dashed lines, PCM model added. The symbols identify four different frames; thick lines represent averages over 40 snapshots.

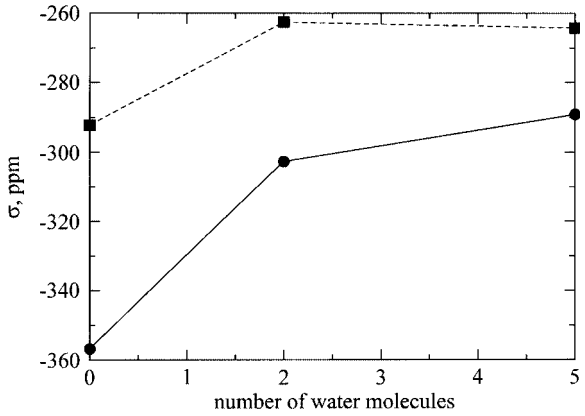

Figure 9. Acetone absolute ^{17}O shielding computed at the PBE0/6–311+G(d,p) level on 40 snapshots extracted from classical dynamics, as a function of the number of explicit water molecules retained in the NMR calculation. Full line, NMR calculated *in vacuo* on the acetone–water clusters; dashed line, PCM model added.

Of course, the quality of the simulation also has an impact on the calculated NMR parameters. From comparison with the results of an *ab initio* Car–Parrinello simulation (with the PBE functional) of the acetone–water mixture, and also with static DFT computations on cluster energies and geometries, it became apparent that to reproduce correctly the angular distribution function of the water oxygen around the carbonyl oxygen an *ad hoc* reparametrization of the AMBER force field was needed, the crucial modifications being a reproduction of the PBE rather than the experimental geometry of acetone, and introduction of explicit lone pairs on the carbonyl oxygen. Figure 10 allows a visual comparison between the distribution of the water oxygens (belonging to water molecules hydrogen-bonded to acetone), as obtained from simulations using the two force fields. After the modification, the agreement with the Car–Parrinello simulation becomes satisfactory.

The convergence of computed NMR parameters with respect to cluster size, etc., was basically unaffected with respect to the results reported before: two explicit water molecules were sufficient, provided that the PCM model was used. However, the overestimation of the C=O bond length at the PBE level (by about 0.02 Å) leads to a corresponding overestimation of the ^{17}O solvation shift (95.5 ppm by Car–Parrinello simulation, 101.5 ppm by AMBER molecular dynamics, vs an experimental value of 75.5 ppm). When the results are properly corrected for this geometry effect, satisfactory agreement with experiment is restored (e.g. 73.5 ppm by Car–Parrinello simulation).

Integrated QM/MM approaches for the study of large systems

Despite the good scaling properties of DFT methods, the computation of NMR parameters for large molecules of biological interest by a brute-force approach is still out of reach. In such circumstances, a useful strategy that allows for both the large number of atoms and the accuracy of the method employed is based on hybrid models.[28,29] The idea behind this approach is to mix quantum mechanics (QM) and molecular mechanics (MM) descriptions in different parts of the same molecule, and/or to treat different regions of the system with different levels of theory (QM/QM). In this way, the most important parts of the molecule, i.e. the reaction centre or the atoms whose properties are studied and the atoms interacting with them, can be computed by an expensive QM methodology, whereas other parts of the molecule, containing well-parametrized atoms and simple interactions are treated at the MM level.

The key steps of this approach are the assessment of a suitable partition pattern and the saturation of the dangling bonds originating from the breaking of covalent bonds in the definition of the model system. Only recently have hybrid methods been applied to calculate magnetic properties in organic molecules[47] and biological systems.[29,48] Here we shall consider in detail the case of the bicyclic homodetic nonapeptide BCP2 shown in Fig. 11, and designed to study the structural requirements for calcium binding peptides.[49]

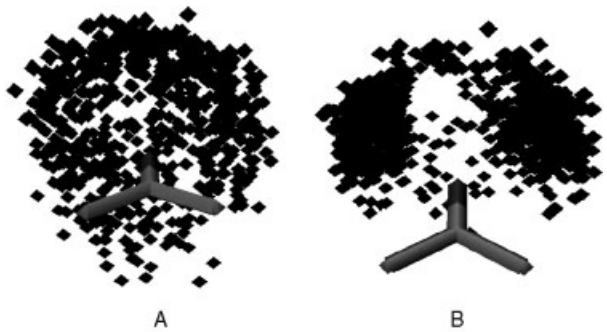

Figure 10. Angular distribution of water oxygen atoms around the carbonyl, resulting from molecular dynamics carried out with the original (A) and the optimized (B) force field.

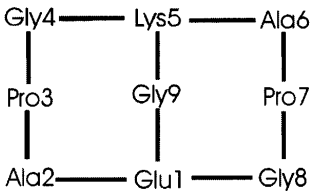

Figure 11. Sequence of BCP2 peptide.

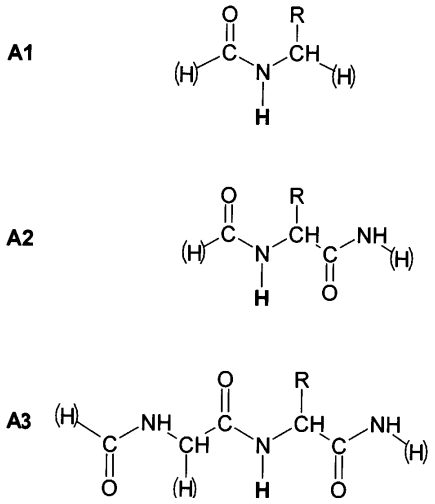

Figure 12. QM region of partition schemes S1, S2 and S3.

^{1}H NMR spectra of the free peptide exhibit sets of signals corresponding to at least four conformers at an intermediate exchange rate, while the presence of a metal cation forces the binding peptide into a rigid conformation, which has been determined through proton NMR studies.[50] Our aim is to set up a protocol for the evaluation of the magnetic shielding of amide protons in the peptide. In particular, three different partition schemes (schemes S1, S2 and S3) are tested within a QM/MM hybrid framework: each scheme is made up of an inner region (or layer) which is treated at QM level, while atoms in the remaining part of the molecule are described as point charges, obtained from AMBER[27] parameters. In each partition scheme (see Fig. 12), QM regions (called fragments A1–A3, respectively) are centered on the nucleus under investigation (amidic hydrogen).

To ensure that the model system has the same electronic structure as the real system, hydrogen atoms are employed to saturate dangling bonds and the original bond distance is scaled by 0.7 in order to resemble a C—H bond length.

In the first fragmentation, only the amidic moiety N_iH and the vicinal groups $C'_{i-1}O$ and C_iR, where R indicates the peptidic side-chain, are included in the QM region and link atoms are introduced between C_i and C'_i and between C'_{i-1} and C_{i-1}. The QM fragment in S2 is extended along the peptide backbone to include the successive peptidic bond between C'_i and N_{i+1}. Finally, the third partition scheme contains both the peptidic bonds preceding and following the nucleus of interest. Link atoms are used between C'_{i-2} and C_{i-2} and between N_{i+1} and C_{i+1}.

Table 6 shows chemical shielding constants calculated for fragments A1, A2 and A3, at the QM level, and using the QM/MM approach (schemes S1–S3); it is apparent that fully converged results are obtained using scheme S3.

We evaluated differences in chemical shieldings computed for different schemes (Δ_{S1-S2} and Δ_{S2-S3}). Whereas Δ_{S1-S2} is more or less constant, significant differences are found for Δ_{S2-S3}, concerning residues Ala2, Gly4 and Gly8 (Δ_{S2-S3} = 2.8, 1.7 and 2.1 ppm, respectively). This could be related to the fact that, on going from partition scheme S2 to S3, the carbonyl moiety involved in the H-bond with H^N shifts from the MM to the QM region. To confirm this hypothesis, we tested an Ala2 model in which the QM region A3 has been replaced by fragment A2, and either formaldehyde or formamide are used to mimic the acceptor group of the H-bond. In the former case Δ_{S2-S3} = 1.7 ppm, whereas in the latter Δ_{S2-S3} = 2.6 ppm. The latter result is very close to the value for partition scheme S3 (2.8 ppm).

The effect due to AMBER charges is significant only for those residues in which H^N is involved in hydrogen bonds (Ala2, Gly4 and Gly8), and for partition schemes S1 and S2, where the QM region is relatively small. Even in these cases convergence is reached with partition scheme S3.

Side-chains are expected to have a minor influence on the chemical shift of amidic hydrogen atoms. We therefore modified partition scheme S3 by treating the side-chains at the MM level, i.e. substituting the β-carbon atoms of Glu1,

Table 6. NMR chemical shieldings (ppm) calculated using three different partition schemes at QM level (2nd, 4th and 6th columns), with the QM/MM method (3rd, 5th and 7th columns) and with the final QM/QM/MM approach (9th column); comparisons for hybrid methods are with full QM calculations at the HF/6–31G(d) (8th column) and PBE0/6–311+G(2d,p) levels (10th column), respectively

Residue	A1	S1	A2	S2	A3	S3	BCP2 HF/6–31G(d)	QM/QM/MM[a]	BCP2 PBE0/6–311+G (2d,p)
Glu1	28.5	28.4	27.2	27.5	27.4	27.2	27.6	25.6	25.9
Ala2	28.4	26.6	27.3	25.9	24.5	24.4	24.5	22.8	22.8
Gly4	29.0	27.4	28.5	27.4	26.8	26.6	26.6	24.8	25.0
Lys5	28.7	29.2	27.8	28.2	27.4	27.8	27.5	26.2	26.0
Ala6	28.7	28.4	27.7	27.3	26.8	27.0	26.7	25.6	25.9
Gly8	28.8	27.0	28.0	26.8	25.9	25.7	25.6	23.8	24.0
Gly9	28.8	29.1	28.3	28.4	28.0	27.6	27.5	26.6	26.0

[a] ONIOM-like procedure: A1 by PBE0/6–311+G(2d,p), A3 by HF/6–31G(d), remaining atoms as point charges.

Ala2, Lys5 and Ala6 by link atoms. The results show that side-chains can be neglected for alanine residues, whereas they play an important role in longer chain amino acids such as Glu1 and Lys5. This is easy to understand, as the side-chains of Glu1 and Lys5 are involved in the bridge of the bicyclic peptide.

The above test and observations show that a fairly large QM region is needed to obtain a good agreement with full QM results and this limits, of course, the sophistication of the QM model. On the other hand, we have already pointed out that a correlated method is needed to compute shieldings for heavy atoms comparable to experimental results. In order to take into account these seemingly opposite requirements, we tested a three-layer QM/QM/MM hybrid method, in which two different QM approaches are used in an ONIOM-like scheme[28,51] and point charges take into account polarization due to the remaining part of the molecule. Figure 13 shows the three different layers in which the system is divided: the innermost layer (rendered by balls and sticks) corresponds to the A1 fragment, whereas the intermediate QM model (represented by tubes in Fig. 13) is equivalent to the A3 fragment. The former layer is described at the PBE0/6–311+G(2d,p) level, whereas the latter layer is treated at the HF/6–31G(d) level, allowing the MM charges to polarize the HF wavefunction. In this case three separate calculations are performed and the expression for the isotropic NMR chemical shielding becomes $\sigma_{iso} = \sigma_{iso}(HF/MM,A3) + \sigma_{iso}(DFT,A1) - \sigma_{iso}(HF,A1)$, namely the DFT value in the small fragment is corrected by the polarization effect obtained at the HF level including the electrostatic embedding by MM charges.

The NMR chemical shieldings of amidic hydrogens calculated using the QM/QM/MM method described above are shown in Table 6 (column 9), together with the reference values computed for the whole peptide at the PBE0/6–311+G(2d,p) level (column 10). The remarkable accuracy of the QM/QM/MM results is apparent and the limited dimensions of the region treated at the DFT level make the whole procedure very effective also for larger systems. In fact, the proposed QM/QM/MM partition leads to a reduction in computer time of about an order of magnitude with respect to a two-layer QM/MM model and of two orders of magnitude with respect to a full QM model.

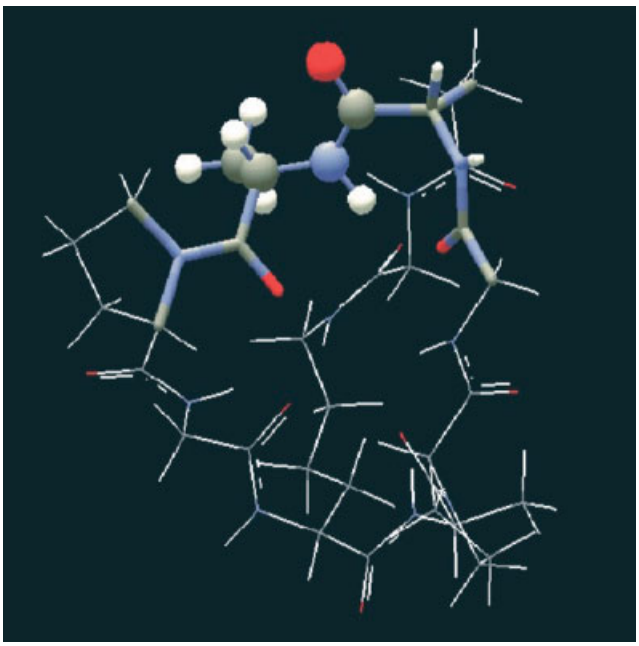

Figure 13. Example of three-layer QM/QM/MM partition scheme. The DFT region is rendered by balls and sticks, the HF region by tubes and the MM region by sticks.

CONCLUSION

This paper is devoted to the analysis of the different factors that play a role in the computation of reliable NMR chemical shifts for molecules in condensed phases. We have first shown that the PBE0 functional coupled to appropriate basis sets provides accurate results for different nuclei (^{1}H, ^{13}C, ^{15}N, ^{17}O) in small molecules and that its favourable scaling properties allow for the direct study of relatively large systems with comparable accuracy. Next, we have shown that the PCM approach allows for an effective introduction of bulk solvent effects, which can be completed, for polar groups in hydrogen-bonding solvents, by explicit treatment of first-shell solvent molecules. The resulting discrete/continuum model is very powerful and can be used also in a dynamic context, resorting to classical or Car–Parrinello simulations. Despite their computational efficiency, brute-force DFT computations of true biological systems are not always feasible. We have shown, using the example of a cyclic polypeptide, that in these cases integrated QM/QM/MM methods can be profitably used, provided that the fragmentation pattern is chosen carefully.

In summary, although further developments are needed to increase the reliability and efficiency of the different parts of the integrated computational tool we have described, it already represents a very powerful aid for the assignment and interpretation of NMR spectra in terms of structure–property relationships.

Acknowledgments

This work was supported by the Italian Ministry of Instruction, University and Research (MIUR). We thank the Sezione di Modellistica Computazionale of the CIMCF (Università Federico II, Naples) for technical support.

REFERENCES

1. Osapay K, Case DA. *J. Am. Chem. Soc.* 1991; **113**: 9436.
2. Kuntz ID, Kosen PA, Craig EC. *J. Am. Chem. Soc.* 1991; **113**: 1406.
3. Asakura T, Taoka K, Demura M, Williamson MP. *J. Biomol. NMR* 1995; **6**: 227.
4. Helgaker T, Jaszunski M, Ruud K. *Chem. Rev.* 1999; **99**: 293.
5. Oldfield E. *Annu. Rev. Phys. Chem.* 2002; **53**: 349.
6. Koch W, Holthausen MC. *A Chemist's Guide to Density Functional Theory*. Wiley-VCH: Weinheim, 2000.
7. Adamo C, di Matteo A, Barone V. *Adv. Quantum Chem.* 1999; **36**: 45.
8. Cheeseman JR, Trucks GW, Keith TA, Frisch MJ. *J. Chem. Phys.* 1996; **104**: 5497.
9. Malkin VG, Malkina OL, Casida ME, Salahub DR. *J. Am. Chem. Soc.* 1994; **116**: 5898.
10. Rauhut G, Puyear S, Wolinski K, Pulay P. *J. Phys. Chem.* 1996; **100**: 6130.
11. Adamo C, Barone V. *J. Chem. Phys.* 1999; **110**: 6158.

12. Allen MJ, Keal TW, Tozer DJ. *Chem. Phys. Lett.* 2003; **380**: 70.
13. Adamo C, Barone V. *Chem. Phys. Lett.* 1998; **298**: 113.
14. Improta R, Barone V. *Chem. Rev.* 2004; **104**: 1231.
15. Frisch MJ, Trucks GW, Schlegel HB, Scuseria GE, Robb MA, Cheeseman JR, Montgomery JA Jr, Vreven T, Kudin KN, Burant JC, Millam M, Iyengar SS, Tomasi J, Barone V, Mennucci B, Cossi M, Scalmani G, Rega N, Petersson GA, Nakatsuji H, Hada M, Ehara M, Toyota K, Fukuda R, Hasegawa J, Ishida M, Nakajima T, Honda Y, Kitao O, Nakai H, Klene M, Li X, Knox JE, Hratchian HP, Cross JB, Adamo C, Jaramillo J, Gomperts R, Stratmann RE, Yazyev O, Austin AJ, Cammi R, Pomelli C, Ochterski JW, Ayala PY, Morokuma K, Voth GA, Salvador P, Dannenberg JJ, Zakrzewski VG, Dapprich S, Daniels AD, Strain MC, Farkas O, Malick DK Rabuck AD, Raghavachari K, Foresman JB, Ortiz JV, Cui Q, G. Baboul G, Clifford S, Cioslowski J, Stefanov BB, Liu G, Liashenko A, Piskorz P, Komaromi I, Martin RL, Fox DJ, Keith T, Al-Lahman MA, Peng CY, Nanayakkara A, Challacombe M, Gill PMW, Johnson B, Chen W, Wong MW, Gonzalez C, Pople JA. *Gaussian 03, Revision B.05*. Gaussian: Pittsburgh, PA, 2003.
16. Perdew JP, Burke K, Ernzerhof M. *Phys. Rev. Lett.* 1996; **77**: 3865.
17. (a) Becke AD. *Phys. Rev. A* 1988; **38**: 3098; (b) Lee C, Yang W, Parr RG. *Phys. Rev. B* 1988; **37**: 785; (c) Becke AD. *J. Chem. Phys.* 1993; **98**: 5648.
18. (a) Hariharan PC, Pople JA. *Theor. Chim. Acta* 1973; **28**: 213; (b) Krishnan R, Binkley JS, Seeger R, Pople JA. *J. Chem. Phys.* 1980; **72**: 650; (c) Francl MM, Pietro WJ, Hehre WJ, Binkley JS, Gordon MS, DeFrees DJ, Pople JA. *J. Chem. Phys.* 1982; **77**: 3654.
19. Dunning TH Jr. *J. Chem. Phys.* 1989; **90**: 1007.
20. (a) Barone V, Cossi M, Tomasi J. *J. Chem. Phys.* 1997; **107**: 3210; (b) Cossi M, Barone V. *J. Chem. Phys.* 2001; **115**: 4708.
21. (a) Cossi M, Scalmani G, Rega N, Barone V. *J. Chem. Phys.* 2002; **117**: 43; (b) Scalmani G, Barone V, Kudin KN, Pomelli CS, Scuseria GE, Frisch MJ. *Theor. Chem. Acc.* 2004; **111**: 90.
22. Car R, Parrinello M. *Phys. Rev. Lett.* 1985; **55**: 2471.
23. Giannozzi P, De Angelis F, Car R. *J. Chem. Phys.* 2004; **120**: 5903.
24. (a) Pasquarello A, Laasonon K, Car R, Lee C, Vanderbilt D. *Phys. Rev. Lett.* 1992; **69**: 1982; (b) Laasonon K, Pasquarello A, Car R, Lee C, Vanderbilt D. *Phys. Rev. B* 1993; **47**: 10 142.
25. (a) Iyengar SS, Schlegel HB, Millam JM, Voth GA, Scuseria GE, Frisch MJ. *J. Chem. Phys.* 2001; **115**: 10 291; (b) Schlegel HB, Iyengar SS, Li X, Millam JM, Voth GA, Scuseria GE, Frisch MJ. *J. Chem. Phys.* 2002; **117**: 8694.
26. Case DA, Pearlman DA, Caldwell JW, Cheetham TE III, Ross WS, Simmerling CL, Darden TA, Merz KM, Stanton RV, Cheng AL, Vincent JJ, Crowley M, Tsui V, Radmer RJ, Duan Y, Pitera J, Massova I, Seibel GL, Singh UC, Weiner PK, Kollman PA. *Amber6*. University of California: San Francisco.
27. Cornell WD, Cieplak P, Bayly CI, Gould IR, Merz KM Jr, Ferguson DM, Spellmeyer DC, Fox T, Caldwell JW, Kollman PA. *J. Am. Chem. Soc.* 1995; **117**: 5179.
28. (a) Svensson M, Humbel S, Morokuma K. *J. Chem. Phys.* 1996; **105**: 3654; (b) Vreven T, Morokuma K. *J. Comp. Chem.* 2000; **21**: 1419.
29. (a) Bakowies D, Thiel W. *J. Phys. Chem.* 1996; **100**: 10 580; (b) Cui Q, Karplus M. *J. Phys. Chem. B* 2000; **104**: 3721.
30. (a) Bagno A. *Chem. Eur. J.* 2001; **7**: 1652; (b) Bagno A, Rastrelli F, Saielli G. *J. Phys. Chem. A* 2003; **107**: 9964; (c) Giesen DJ, Zumbulyadis N. *Phys. Chem. Chem. Phys.* 2002; **4**: 5498.
31. Hasegawa K, Ueno Y. *Bull. Chem. Soc. Jpn* 1985; **58**: 2832.
32. Crescenzi O, Correale G, Bolognese A, Piscopo V, Parrilli M, Barone V. 2004; **2**: 1577.
33. Napolitano A, Crescenzi O, Camera E, Giudicianni I, Picardo M, d'Ischia M. *Tetrahedron* 2002; **58**: 5061.
34. Krohn BJ, Ermler WC, Kern CW. *J. Chem. Phys.* 1974; **60**: 22.
35. Ruden TA, Lutnaes OB, Helgaker T, Ruud K. *J. Chem. Phys.* 2003; **118**: 9572.
36. Aastrand P-O, Ruud K, Taylor PR. *J. Chem. Phys.* 2000; **112**: 2655.
37. (a) Vaara J, Lounila J, Ruud K, Helgaker T. *J. Chem. Phys.* 1998; **109**: 8388; (b) Ruud K, Aastrand P-O, Taylor PR. *J. Chem. Phys.* 2000; **112**: 2668.
38. Ruff O, Heinzelmann A. *Z. Anorg. Allg. Chem.* 1911; **72**: 63.
39. Taha AN, True NS, LeMaster CB, LeMaster CL, Neugebauer-Crawford SM. *J. Phys. Chem. A* 2000; **104**: 3341.
40. Adamo C, Cossi M, Rega N, Barone V. In *Theoretical Biochemistry: Processes and Properties of Biological Systems. Theoretical and Computational Chemistry*, vol. 9, Eriksson LA (ed.). Elsevier: New York, 2001; 467–538.
41. Barone V, Crescenzi O, Improta R. *Quant. Struct.–Act. Relat.* 2002; **21**: 105.
42. Schlegel HB. *Bull. Korean Chem. Soc.* 2003; **24**: 837.
43. Piana S, Sebestiani D, Carloni P, Parrinello M. *J. Am. Chem. Soc.* 2001; **123**: 8730.
44. Malkin VG, Malkina OL, Steinebrunner G, Huber H. *Chem. Eur. J.* 1996; **2**: 452.
45. Cossi M, Crescenzi O. *J. Chem. Phys.* 2003; **118**: 8863.
46. Jorgensen WL, Chandrasekhar J, Madura JD, Impey RW, Klein ML. *J. Chem. Phys.* 1983; **79**: 926.
47. Karadakov PB, Morokuma K. *Chem. Phys. Lett.* 2000; **317**: 589.
48. Molina PA, Sikorski RS, Jensen JH. *Theor. Chem. Acc.* 2003; **109**: 100.
49. Di Blasio B, Benedetti E, Pavone V, Pedone C, Saviano M, Zanotti G, Blout ER. *Biopolymers* 1990; **30**: 509.
50. Oliva R, Falcigno L, D'Auria G, Zanotti G, Paolillo L. *Biopolymers* 2001; **56**: 27.
51. Svensson M, Humbel S, Froese RDJ, Matsubara T, Sieber S, Morokuma K. *J. Phys. Chem.* 1996; **100**: 19 357.